Journal of Groundwater Science and Engineering
ISSN 2305-7068
Indexed by ESCI CABI CSA
Scopus GeoRef AJ CNKI

Research on the characteristics and influencing factors of terrestrial heat flow in Guizhou Province

Shuai-chao Wei, Feng Liu, Wei Zhang, Gui-ling Wang, Ruo-xi Yuan, Yu-zhong Liao, Xiao-xue Yan

Citation:
Wei SC, Liu F, Zhang W, *et al*. 2022. Research on the characteristics and influencing factors of terrestrial heat flow in Guizhou Province. Journal of Groundwater Science and Engineering, 10(2): 166-183.

View online: https://doi.org/10.19637/j.cnki.2305-7068.2022.02.006

Journal of Groundwater Science and Engineering 10(2022) 166–183

Journal homepage: http://gwse.iheg.org.cn

Research on the characteristics and influencing factors of terrestrial heat flow in Guizhou Province

Shuai-chao Wei[1,2], Feng Liu[1,2,3], Wei Zhang[1,2], Gui-ling Wang[1,2*], Ruo-xi Yuan[1,2], Yu-zhong Liao[1,2], Xiao-xue Yan[1,2]

[1] *Institute of Hydrogeology and Environmental Geology, Chinese Academy of Geological Sciences, Shijiazhuang* 050061, *China*.
[2] *Technology Innovation Center of Geothermal & Hot Dry Rock Exploration and Development, Ministry of Natural Resources, Shijiazhuang* 050061, *China*.
[3] *China University of Geosciences (Beijing), Beijing* 100083, *China*.

Abstract: Terrestrial heat flow is an important physical parameter in the study of heat transfer and thermal structure of the earth and it has great significance in the genesis and development and utilization potential of regional geothermal resources. Although several breakthroughs in geothermal exploration have been made in Guizhou Province. The terrestrial heat flow in this area has not been properly measured, restricting the development of geothermal resources in the province. For this reason, the terrestrial heat flow in Guizhou was measured in this study, during which the characteristics of heat flow were determined using borehole thermometry, geothermal monitoring and thermal property testing. Moreover, the influencing factors of the terrestrial heat flow were analyzed. The results show that the thermal conductivity of rocks ranges from 2.0 W/(m·K) to 5.0 W/(m·K), with an average of 3.399 W/(m·K); the heat flow varies from 30.27 mW/m^2 to 157.55 mW/m^2, with an average of 65.26 ± 20.93 mW/m^2, which is slightly higher than that of the average heat flow in entire land area in China. The heat flow in Guizhou generally follows a dumbbell-shaped distribution, with high values present in the east and west and low values occurring in the north and south. The terrestrial heat flow is related to the burial depths of the Moho and Curie surface. The basaltic eruptions in the Emeishan led to a thinner lithosphere, thicker crust and lateral emplacement, which dominated the basic pattern of heat flow distribution in Guizhou. In addition, the dichotomous structure of regional active faults and concealed deep faults jointly control the heat transfer channels and thus influence the terrestrial heat flow.

Keywords: Thermal conductivity; Terrestrial heat flow; Moho; Curie surface; Emeishan basaltic

Received: 26 Aug 2021/ Accepted: 02 Apr 2022

Introduction

The terrestrial heat flow (heat flow in short) directly reflects the thermal processes inside the Earth (Wang and Huang, 1990; Jiang et al. 2019; Yang et al. 2020; Zhang et al. 2021; Chen et al. 2022) and is a fundamental physical parameter for characterizing the heat transfer in the Earth from inside to outside. Moreover, the heat flow is one of the most critical parameters for study of regional geothermal fields, lithospheric thermal structures and tectonic evolution, and for geothermal resources assessment (Wang et al. 2021; He, 2015; Furlong and Chapman, 2013; Rolandone et al. 2013; Grall et al. 2012; Zhang et al. 2019; Wang et al. 2020; Li et al. 2021). In the case of one-dimensional steady-state conduction, heat flow is calculated by multiplying the average rock thermal conductivity of the cross section and the average geothermal gradient of that section (Wang, 2015; Liu et al. 2020a).

Wang et al. (1990) carried out the earliest study on the heat flow in Guizhou Province, obtaining estimated heat flow of 29.3–58.45 mW/m^2 in 24 boreholes, with an average of 45.95 mW/m^2, which can roughly reflect the regional geothermal conditions. A study by Yuan et al. (2006) suggest that Guizhou is in the middle-low temperature geoth-

*Corresponding author: Gui-ling Wang, *E-mail address*: guilingw@163.com

DOI: 10.19637/j.cnki.2305-7068.2022.02.006

Wei SC, Liu F, Zhang W, et al. 2022. Research on the characteristics and influencing factors of terrestrial heat flow in Guizhou Province. Journal of Groundwater Science and Engineering, 10(2): 166-183.

ermal gradient zone, the geothermal gradient is 20–25℃/km and heat flow is 40–60 mW/m^2. Heat flow was found to be high in the west and low in the east, while Xing et al. (2007) reported a slightly lower range of 30–50 mW/m^2. Until now, only two measured heat flow points have been published in Guizhou, both of which are in Guiyang city and the heat flow was measured at 63.40 mW/m^2 and 67.19 mW/m^2, respectively (Wu et al. 2012).

In recent years, Guizhou has been actively promoting itself as the "Hot Spring Province of China". The amount of geothermal exploration and the number of geothermal wells in the province have been increasing, offering great potential for the development and utilization of geothermal resources. Many studies have been conducted on geothermal exploration technology and theory (Wang and Wang, 2007; Lu et al. 2013; Zhang et al. 2014; Duan et al. 2015; Yang et al. 2018; Ban et al. 2018; Zhu, 2020), but most of them are limited to a site scale and do not cover the whole province. As a result, the heat flow of most areas in Guizhou has not previously been measured (Jiang et al. 2016). This gap has restricted the study of geothermal resource exploration and distribution patterns in the province. In 2020, the project team of the project entitled *National Geothermal Heat Flow Value Measurement and Target Area Selection* organized by the China Geological Survey carried out heat flow measurements in Guizhou. In this study, borehole temperatures, collected rock samples were measured, and thermal property tests of rocks were conducted across the province. Then, based on the collected data and measurements, the heat flow values were compiled and analyzed, and a primary distribution map of heat flow was generated in Guizhou Province. Finally, this study analyzed the influencing factors of the heat flow and made suggestions regarding the key areas of the future exploration and research on geothermal resources in Guizhou.

1 Regional geothermal geological characteristic

Guizhou is located at the intersection of the Upper Yangtze Block and the Jiangnan Orogenic Belt (Fig. 1a). Since the Neoproterozoic, Guizhou has undergone several phases of tectonic activities. Influenced by the Tethys Tectonic Domain and the Jiangnan Orogenic Belt, deep structures have controlled the paleogeographic pattern, tectonic unit delineation, geological evolution and context of mineralization in the region (Wang et al. 2021; Dai et al. 2013). Active faults have mainly developed in the north-west, north-east and nearly-north-south directions. Among them, the Pu'an-Guiyang-northern Fanjingshan fault zone divides the Upper Yangtze Block and the Jiangnan Orogenic Belt. There are obvious differences in geological setting, geophysics, and geochemistry on both sides of the fault zone (GSGP, 2017). A relatively complete strata has developed in Guizhou and all strata from the Neogene to the Quaternary are exposed. The outcrops mainly consist of sedimentary rocks dominated by carbonates and epimetamorphic sedimentary rocks dominated by greenschist facies, followed by a few igneous and deeply metamorphic rocks. Among these outcrops, carbonates are the most widely distributed, accounting for about 61.9% of the province's area (GSGP, 2017).

Hydrocensus show that there are currently a total of 212 hot springs and geothermal wells in Guizhou, including 36 geothermal wells, 84 exploitable geothermal wells, and 92 artesian hot springs (Fig. 1b; Wang et al. 2018). In addition, hot springs of 20–24℃ account for 16% of the province's geothermal resources, 25–40℃ account for 52%, 40–60℃ account for 31%, and 60–90℃ account for only 1%. Most of the hot springs fall in the warm water category in low-temperature geothermal resources (Yang et al. 2015). According to the tectonic genesis, there are two types of underground geothermal water in Guizhou: Uplifted mountain type and sedimentary basin type. The former is more widely distributed in the province and mainly consists of two types of folded zones in terms of tectonic style, namely the Jura and Jiangnan types. The latter is distributed in Chishui and Xishui areas in Guizhou. High temperature contributes to the horizontal circulation of groundwater in the Permian and Triassic carbonate rocks, leading to the formation of thermal brines associated with oil and gas (Wang et al. 2018).

2 Sampling and tests

Geothermal logging and monitoring were carried out in 85 boreholes. The JGS-1B intelligent engineering logging instrument produced by the Chongqing Geological Instrument Factory was used for geothermal logging. It has a measurement range of 0.1–80℃ and an accuracy of 0.5℃. The geothermal monitoring was carried out using a TD-016C geothermal monitoring system manufactured by Beijing Hongou Chengyun Instrument and Eq-

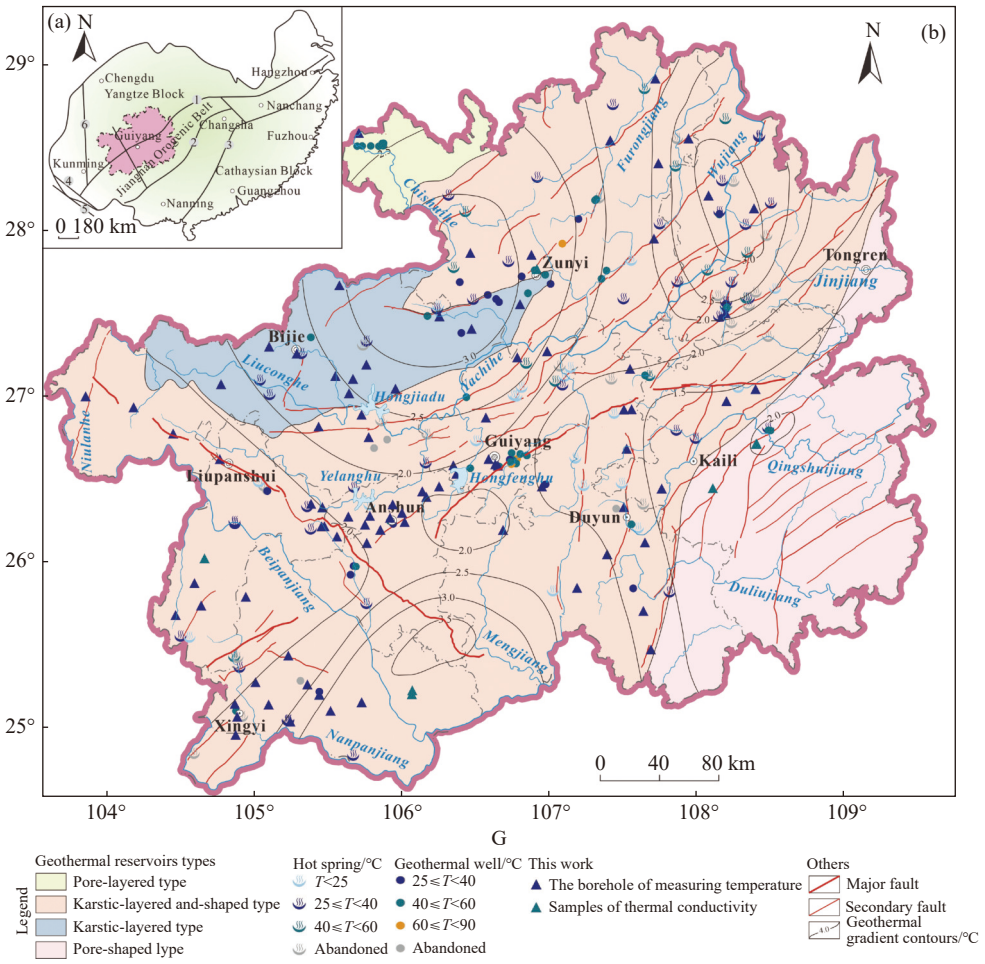

Fig. 1 (a) Map showing the geotectonic location of Guizhou Province (modified from Dai et al. 2013); (b) Geological map showing geothermal resources in Guizhou Province (modified from Wang et al. 2018)

Notes: ① Shizong-Songtao-Cili-Jiujiang fault belt; ② Luocheng-Longsheng-Taojiang-Jingdezhen fault belt; ③ Beihai-Pingxiang-Shaoxing fault belt; ④ Honghe fault belt; ⑤ Ailaoshan fault belt; ⑥ Xiaojiang fault belt

uipment Co., Ltd, which has a measurement range of 0–90℃, a resolution of 0.05℃, and an accuracy of 0.2℃ (Liu et al. 2020a). The temperature measurements were carried out when the borehole was in steady-state or quasi-steady-state conditions.

A total of 66 thermal conductivity samples in 34 groups were collected from the Upper Paleozoic to Triassic strata. They are composed of siliceous tuff, marl, tuff, muddy dolomite, dolomite, siltstone, siltstone, fine sandstone, metamorphic tuff and slate. All the samples were either borehole cores or rocks collected from the core strata at the ground surface near the boreholes. The samples were collected in Anshun, Zunyi, Bijie, Liupanshui, Xinyi, Duyun, Kaili and Tongren areas in Guizhou (Fig. 1).

The thermal conductivity tests of rocks were performed by the Donghua University of Science and Technology and the Tianjin Rockcord Technology Co., Ltd. using a Thermal Conductivity Scanning (TCS) automatic thermal conductivity scanner made by a Germany company and a flat film thermal analyzer TC3200 made by Xi'an Xiaxi Electronic Technology Co., which have a measurement range of 0.2–25 W/(m·K) and measurement accuracy of 3% (Liu et al. 2020a).

3 Results

3.1 Thermal conductivities of rocks

The test results are shown in Table 1. Most of the thermal conductivities of the collected rocks are within 2.0–5.0 W/(m·K), with an average of 3.399 W/(m·K), a minimum of 1.523 W/(m·K), and a maximum of 5.533 W/(m·K). According to the thermal conductivity statistics of different lithologies, the average of thermal conductivity is in the order of sandy mudstones (2.322 5 W/(m·K)) < siltstones (3.013 W/(m·K)) < marls (3.05 W/(m·K)) < limestones (3.096 (W/(m·K)) < tuffs (3.33 W/

Table 1 Test results of rock thermal conductivity in the study area

Sample	Stratum	Lithology	Thermal conductivity（W/(m·K)）	Error/%
BLC-1	Middle Triassic Banna Fm.	Fine sandstone	4.372	0.7
BLC-2		Sandy mudstone	1.523	0.2
DSC	Middle Triassic Shizishan Fm.	Muddy dolomite	2.776	0.6
GMC	Middle Triassic Guanling Fm.	Limestone	1.901	0.7
DWZ			2.379	0.7
NWC		Dolomite	2.867	0.4
GJC	Lower Triassic Yongningzhen Fm.	Limestone	3.395	0.6
YZYC			3.369	0.4
BJ-1	Lower Triassic Maocaopu Fm.	Muddy tuff	2.806	0.3
BJ-2		Limestone	1.847	0.3
LCQ-1	Lower Triassic Yelang Fm.	Muddy tuff	3.294	0.4
LCQ-2		Limestone	1.965	0.2
LCQ-3		Sandy mudstone	3.122	0.5
LGC		Limestone	3.239	0.5
LCB	Lower Triassic Anshun Fm.	Dolomite	1.986	0.4
QGQC	Upper Permian Changxing Fm.	Limestone	2.323	0.5
PMC	Upper Permian Wujiaping Fm.	Limestone	4.372	0.3
DJ-1	Middle Permian Longtan Fm.	Fine sandstone	3.502	0.8
WD		Siltstone	3.013	0.5
SC-1	Middle Permian Maokou Fm.	Limestone	3.618	0.5
ZK01	Lower Carboniferous Shangsi Fm.	Limestone	3.05 (10)	—
CY	Upper Devonian Yaosuo Fm.	Dolomite	3.305	0.5
PLC		Siliceous tuff	1.591	0.3
KLC		Siliceous tuff	5.533	0.6
LJXC	Lower Ordovician Honghuanyuan Fm.	Limestone	3.277	0.2
ZK02	Upper Cambodian shangsi Fm.	Limestone	4.59 (9)	—
		Dolomite	4.71 (6)	—
ZK03	Upper Cambrian Shilengshui Fm.	Dolomite	4.84 (10)	—
MXC	Upper Cambrian Houba Fm.	Muddy dolomite	5.287	0.6
DCY	Upper Cambodian Gaotai Fm.	Dolomite	5.303	0.4
DBC	Middle and Upper Cambrian Loushanguan Group	Dolomite	3.640	0.1
CWTC			5.197	0.3
JH-2	Lower Cambrian Jindingshan Fm.	Limestone	4.032	0.3
DSP	Upper Proterozoic Qingshuijiang Fm.	Tuff	3.330	0.7
JH-1	Upper Proterozoic Fanshao Fm.	Slate	3.611	0.8

Notes: Number of samples is shown in brackets. Fm.- Formation.

(m·K)) < siliceous limestones (3.562 W/(m·K)) < slates (3.611W/(m·K)) < fine-grained sandstones (3.981W/(m·K)) < dolomites (3.981W/(m·K)) < muddy dolomites (4.031W/(m·K)). In addition, the thermal conductivities of dolomite and chert vary the most, with a wide rage of up to 3.3 W/(m·K). This variation may be due to differences in mineral composition, rock structures and stratigraphy (Song et al. 2019).

The thermal conductivities obtained in this study are basically consistent with those published by Song et al. (2019) in Table 2, while dolomite and tuff have slightly lower values and the rest have slightly higher values than the average value.

Comparing our results with results from the same lithologies in North China (Chen et al. 1988), Northwest China (Wang et al. 1995), and Southeast China (Xiong et al. 1994) (Table 2), it can be found that the present thermal conductivity of mudstones in Guizhou is close to that in Northwest China,

Table 2 Comparison of thermal conductivity statistics of different lithologies with other regions

Lithology	This text W/(m·K)	Guizhou (Song et al. 2019) W/(m·K)	North China (Chen et al.1988) W/(m·K)	Northwest China (Wang et al.1995) W/(m·K)	Southeast China (Xiong et al.1994) W/(m·K)
Siltstone	2.323 (2)	1.806±0.326 (46)	1.97±0.16 (3)	2.506±0.688 (26)	3.59±1.19 (49)
Fine sandstone	3.013 (1)	3.362±0.536 (30)	2.51±0.71 (17)	1.811±0.578 (21)	3.41±1.22 (181)
Dolomite	3.981 (8)	4.540±0.823 (60)	4.34±1.33 (45)	3.501±0.922 (4)	3.30±0.67 (8)
Limestone	3.096 (14)	2.868±0.256 (30)	2.86±1.13 (21)	3.192±0.724 (28)	3.33±0.56 (56)
Muddy tuff	3.050 (2)	2.699±0.259 (28)	1.79±0.10 (1)	—	1.85±0.49 (7)
Tuff	3.330 (1)	3.355±0.378 (30)	—	—	3.36±0.56 (63)
Slate	3.611 (1)	3.040±0.488 (30)	—	—	—

Notes: Number of samples is shown in brackets

higher than that in North China, and lower than that in Southeast China. The thermal conductivities of siltstones and tuffs in Guizhou are close to those in Southeast China and higher than those in North and Northwest China. The thermal conductivities of marls in Guizhou are significantly higher than those in North China and Southeast China. In addition, the thermal conductivities of dolomites and tuffs in Guizhou are close to those in North China and higher than those in Northwest China and Southeast China.

3.2 Measurement and distribution of heat flow

To calculate the heat flow, the following equation was used to determine the heat flow density q under one-dimensional steady-state heat transfer conditions (Liu et al. 2020b):

$$q = -K\frac{dT}{dZ} \tag{1}$$

Where: q is the density of heat flow (mW/m^2), – indicating that the direction of q is vertically upward; $\frac{dT}{dZ}$ is the geothermal gradient (℃/km); K is the thermal conductivity (W/(m·K)) of rocks in the measured well section.

After obtaining the geothermal gradient of the borehole and the thermal conductivity of rocks in the measured well section, the heat flow was estimated using the segmentation method (Liu et al. 2020a) as follows:

$$Q = \sum_{i=1}^{n}\frac{Q_i Z_i}{Z} = \sum_{i=1}^{n}\frac{\Delta T_i K_i}{Z_i}\frac{Z_i}{Z} \tag{2}$$

Where: Q is the total heat flow; Q_i is the heat flow at a measured section Z_i; $\Delta T_i/Z_i$ is the product of the geothermal gradientand, K_i is the thermal conductivity of the measured section; Z is the total length of all measured sections.

In the real condition, the logging curves will show up-concave and down-convex jagged fluctuations because of the groundwater movement and the difference in thermal properties across the tectonic interface in Fig. 2 (Zhang et al. 2020; Mao et al. 2019). To identify the segment that reflects the changes in the formation temperature, it is necessary to screen out the pure heat conduction segment from the curve, where the temperature linearly increases with depth. The actual geothermal gradients can then be estimated using linear fitting method. The approach was applied on the temperature curve of 43 boreholes that can roughly represent the geothermal fields in the study area (GBBGMEDGP, 2015; Ban et al. 2018; Tu et al, 2019; Chen et al. 2014; Hou, 2016; Wu et al. 2012; Tian, 2016; Yuan, 1997; Song et al. 2012; Fang et al. 2020; Zhang and Li, 2015; Lu et al. 2013; Ding et al. 2019; Mu and Wu, 2021). The coefficient of determination (R^2) is used to assess the goodness of the fit. When R^2 >0.95, the temperature curve of the selected section is considered representative of the geothermal characteristics of the borehole area, and the geothermal gradients obtained under these conditions can be used to calculate heat flow.

The rock thermal conductivity was from the present measured data or previously published data (Guo et al. 2018; Song et al. 2019; Lu, 2014), and the heat flow was calculated using the segmentation method. The heat flow values are shown in Table 3. The temperature data from the boreholes Wuchuan ZK02, Karo, and Minxing in this study have high quality. The heat conductivities of the cores of these three wells were used to calculate the heat flow. The quality standard of the resulting heat flow values can reach Class A (Wang et al. 1990). There are four Class A data points in this study. The heat flow values of the boreholes Dongshan, Longgong, Daping, Dongkou, Duijiang and Longjiangqiao reached Class B in terms of quality standard because they were calculated using the

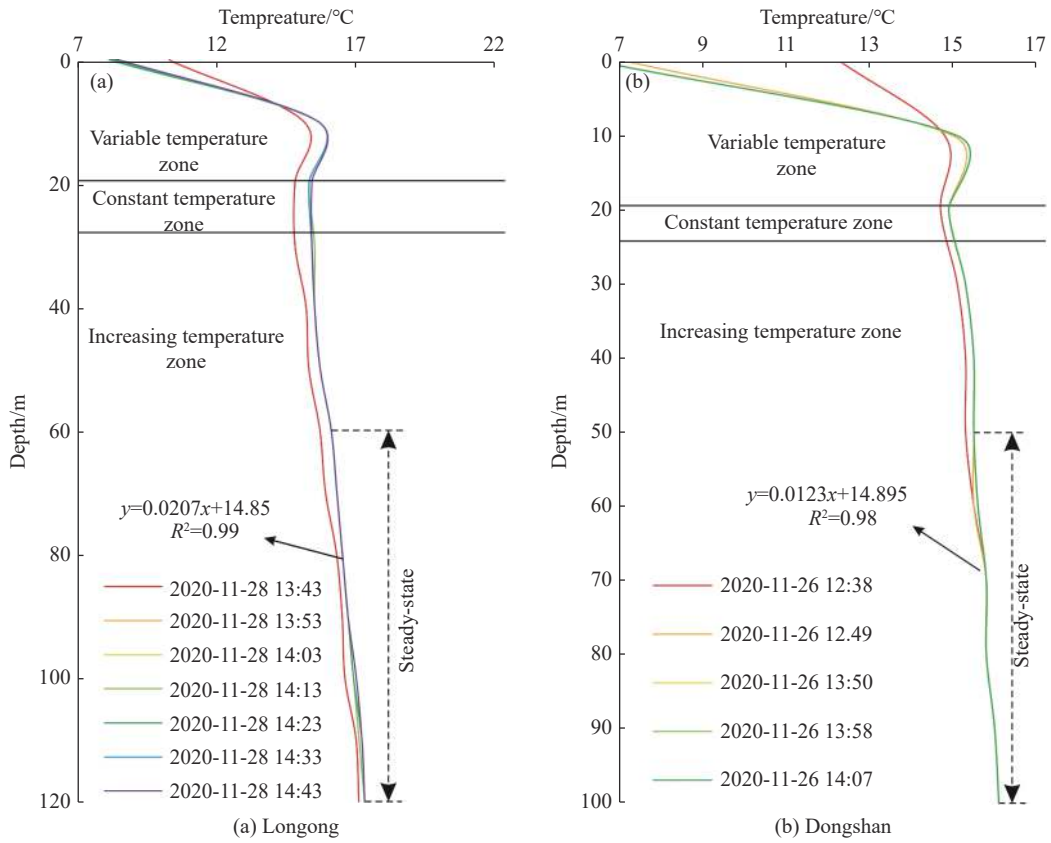

Fig. 2 Temperature curve of ground temperature monitoring

thermal conductivities of the nearby surface rocks corresponding to the lithology at the depths of the boreholes. The heat flow values of boreholes 807, 10–6, 8–1 and 1 109 in the supplementary survey area of Qianxi County also reached Class B since their temperature data have high quality and were calculated using the average thermal conductivity (2.596 W/(m·K)) of siltstones in the Longtan Formation where a linear conduction segment was identified (Guo et al. 2018; Lu, 2014). There are 10 Class B data points in this study. The temperature measurement sections of other boreholes had better data quality, but their heat flow values were calculated using thermal conductivities of nearby surface samples or reference values in the literature and thus fell in Class C in terms of quality standard. As a result, there are 29 Class C data points in this study.

This study updated the thermal conductivities used in previous calculations to be more representative of geological environment. For example, Wu et al. (2012) used the thermal conductivity of the reference borehole (Wang et al. 1990) to calculate the heat flow of boreholes ZK2 and ZK3 in the geothermal field of Wudang District. However, the lithology of the outcrops of the reference borehole is unknown. To improve this, in the current study, the thermal conductivities of the actual lithology of ZK2 and ZK3 were used to calculate the heat flow. The average heat flow values were calculated to be 70.89 mW/m^2 and 79.70 mW/m^2, respectively, which are 5.5% and 25.70% higher than those in the study of Wu et al. (2012) (Fig. 3). Furthermore, both of the newly estimated heat flow are higher than the average value of 62.5 mW/m^2 in China (Hu et al. 2000). This may be explained by the redistribution of heat flow in the core of the Wudang anticline uplift, where the two boreholes are located. The accumulation of heat flow in the uplifted area of the anticline results in higher background heat flow values (Wu et al. 2012).

According to the results, the average heat flow in Guizhou Province is 65.26 ± 20.93 mW/m^2 with a variation range of 30.27–157.55 mW/m^2, and a mode range of 40–80 mW/m^2. The high values above 100 mW/m^2 are located in areas with high-amplitude geothermal gradient anomalies. As shown by the histogram on which the high-amplitude anomalies have been removed, the heat flow is nearly normally distributed (Fig. 4). The histogram also shows that the average heat flow value of Guizhou Province is slightly lower than that of Southeast China of 67.9 mW/m^2 (Xiong et al. 1993), slightly higher than that of the whole land area of China of 62.5 mW/m^2 (Hu et al. 2000), and similar to that of the global land areas of 65 mW/m^2 (Pollack et

Table 3 List of terrestrial heat flow data in Guizhou Province (* is to update the heat flow value)

ID	Longitude	Latitude	Depth (m)	Measuring section (m)	Geothermal gradient (℃/km)	Conductivity W/(m·K)	Staged Heat Flow (mW/m^2)	Mean heat flow (mW/m^2)	Grade	Data source
Dongshan	105.579	27.669	120.60	50–100	12.3	2.776	34.14		B	Measured
Longgong	105.671	27.105	120.10	60–120	20.7	3.239	67.05		B	Measured
Daping	108.390	28.133	107.48	30–80	21.7	3.277	71.11		B	Measured
Karo	107.190	25.843	151.20	60–140	10.2	5.533	56.44		A	Measured
Minxing	107.721	28.917	120.08	50–110	10.0	5.287	52.87		A	Measured
Dongkou	106.003	26.297	120.06	35–105	10.0	4.473	44.73		B	Measured
Duijiang	105.551	27.122	170.00	45–165	13.7	3.502	47.98		B	Measured
Longchang-qiao	105.464	26.330	120.00	40–80	22.0	3.294	72.47		B	Measured
WuchuanZK02	107.946	28.555	306.15	150–225	11.8	5.066	59.78		A	Measured
CK1	107.519	26.240	2 521.56	794.29–1 193.34	15.5	3.085	47.82		C	GBBGMEDGP, 2015
ZK3	108.107	26.395	2 300.00	1 653.83–2 196.21	26.0	2.910	75.66		C	Ban et al. 2018、Tu et al. 2019
ZK2	108.295	26.650	1 618.00	1 017.88–1 603.30	28.2	3.041	85.76		C	
ZK2	105.672	25.903	2 301.00	1 176.2–1 994.8	1.60	2.382	38.11		C	Chen et al. 2014
S-2	104.692	25.992	760.00	452.68–703.32	35.2	3.013	106.06		C	Hou, 2016
ZK2	106.755	26.610	1 922.44	157.65–728.96	21.4	3.277	70.13	73.59*	C	Wu et al. 2012
				1 279.72–1 500	16.3	5.066	82.58			
ZK3	106.751	26.614	2 191.23	214.04–524.08	27.2	3.277	89.13	82.42*	C	
				1 082.62–1 344.43	14.7	5.066	74.47			
ZK5	108.224	27.511	567.00	200–300	31.1	5.066	157.55		C	Tian, 2016
Dongjiu-chang	106.915	27.775	318.00	60–318	15.3	3.277	50.14		C	Yuan,1997
SK08-2	107.653	27.108	1 354.22	850–1 103	23.0	3.330	76.59		C	Duan et al. 2015; Song et al. 2012
CK1	105.303	27.225	2 301.21	1 327–2 204	27.6	4.418	121.94		C	Fang et al. 2020
CK2	105.966	27.270	1 301.30	319–900	19.5	4.032	78.62		C	
ZK1	105.381	27.372	1 934.62	1 231–1 936	13.2	5.066	66.87		C	
ZK4	105.640	27.263	2 471.37	959–1 632	22.1	4.032	89.11		C	
ZK5	105.750	27.012	2 200.07	1 701–2 102	29.5	4.032	118.94		C	

Table3 (continued)

ID	Longitude	Latitude	Depth (m)	Measuring section (m)	Geothermal gradient (℃/km)	Conductivity W/(m·K)	Staged Heat Flow (mW/m^2)	Mean heat flow (mW/m^2)	Grade	Data source
ZK1	106.867	27.631	2 696.00	0–279	23.6	2.320	54.75	65.27	C	Zhang and Li, 2015; Zhang et al. 2014
				279–1 061	16.6	2.670	44.32			
				1 061–1 520	23.9	3.085	73.73			
				1 756–2 675.1	16.2	5.066	82.07			
ZK2	106.944	27.768	3 001.00	0–120	27.5	2.32	63.80	76.81	C	
				120–1 823.5	22.6	4.032	91.12			
				1 823.5–2 362.9	15.2	2.271	34.52			
ZK3	106.921	27.769	3 002.00	0–375	10.4	2.271	23.62	38.05	C	
				375–1 525	12.0	4.032	48.38			
				1 525–2 100	11.8	2.271	26.80			
CK4	107.115	27.929	2 500.00	0–745.16	11.8	5.066	59.78	52.92	C	
				745.16–1 994.66	21.5	2.271	48.83			
CK5	107.029	27.690	2 641.00	0–1 225	11.8	5.066	59.78	52.99	C	
				1 225–1 875	17.7	2.271	40.20			
ZK4	106.524	27.601	1 226.00	0–380	13.1	4.032	52.82		C	
807	105.346	26.655	490.00	105–242	30.2	2.596	78.40		B	Lu et al. 2013; Lu, 2014
10-6	105.339	26.660	893.00	327–527	23.3	2.596	60.49		B	
8-1	105.374	26.655	650.00	200–324	14.7	2.596	38.16		B	
1 109	105.337	26.669	455.00	102–186	30.3	2.596	78.66		B	
Getang	105.297	25.292	—	1 400–1 900	30.0	2.547	76.41		C	Zhu, 2020
ZK001	105.381	25.640	953.00	310–590	27.7	3.382	93.68		C	Ding et al. 2019
ZK705	105.399	25.578	1 364.00	470–990	28.2	3.382	95.37		C	
ZK302	105.413	25.582	1 150.00	300–700	27.1	3.382	91.65		C	
ZK303	105.404	25.571	1 250.00	300–700	26.6	3.382	89.96		C	
ZK402	105.420	25.560	950.00	250–700	27.9	3.382	94.36		C	
ZK1201	105.424	25.550	950.00	300–700	28.9	3.382	97.74		C	
ZK02	108.191	27.470	2 060.37	600–1 320	13.8	4.350	60.03		C	Mu and Wu, 2021

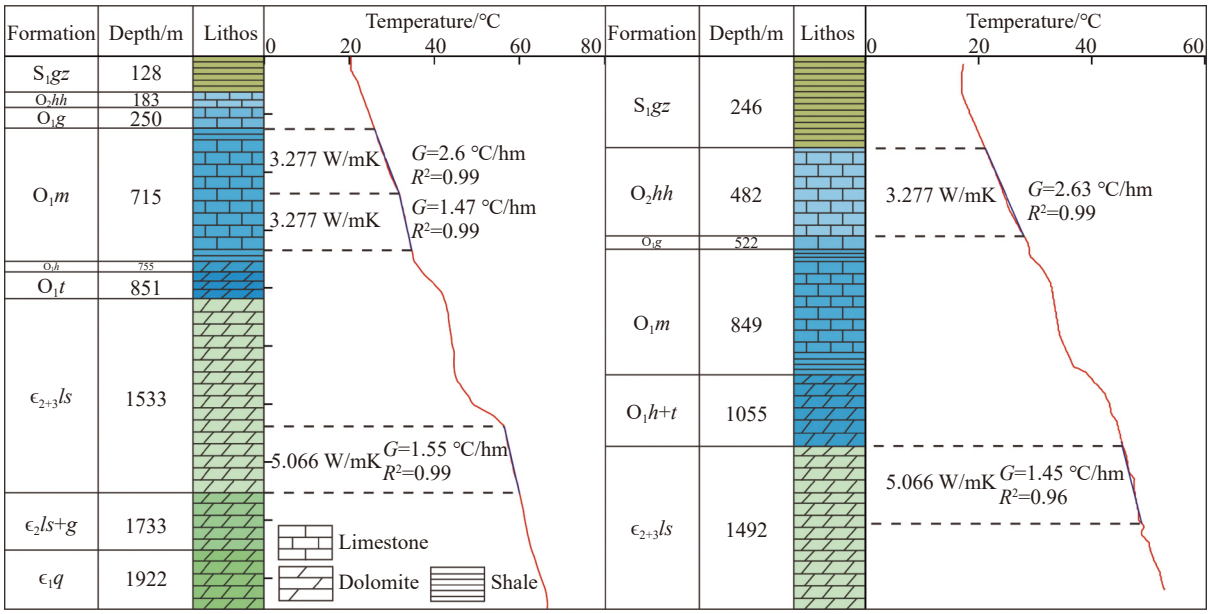

Fig. 3 Stratigraphic column and temperature curve of ZK2 (left) and ZK3 (right) in Wudang geothermal field, Guizhou (modified from Wu et al. 2012)

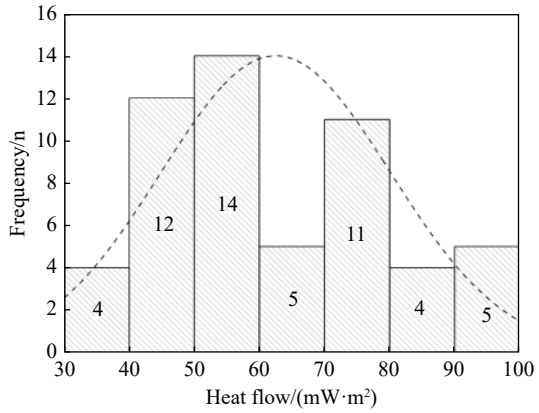

Fig. 4 Histogram of terrestrial heat flow in Guizhou Province

(Notes: >100 mW/m^2 heat flow values account for 5% of the 58 total, not shown on the graph)

al. 1993).

The heat flow contour map (Fig. 5) of Guizhou Province was created using new values from this study combined with existing estimated values (Wang et al. 1990). Fig. 5 shows that the heat flow in Guizhou Province are generally high in the east and west and low in the north and south, following a "dumbbell" distribution. Geographically, the region to the west of the Wangmu-Puding-Qianxi-Dafang area has a significantly high heat flow area with value range of 70–100 mW/m^2. The regions to the east of the Sandu-Leishan- Huangping-Shiqian area and to the south of the Jiangkou-Jinping area are high heat flow areas with values higher than 65 mW/m^2. The region to the north of the Jinsha-Meitan-Dejiang-Jiangkou area is classiefied as a low heat flow area with values generally lower than 65 mW/m^2, and even lower than 50 mW/m^2 in Chishui and Yanhe areas. The regions to the south of the Zhenning-Puding-Guiding-Majiang area, to the west of the Danzhai-Sandu area, and to the east of the Luodian-Guanling area are defined as extreamly low heat flow regions with values much lower than 65 mW/m^2, and only 40 mW/m^2 in the Anshun-Changshun areas.

4 Discussions

4.1 Relationships between geothermal flow and the Moho and the Curie surface

The Moho and Curie surface are important interfaces in the crust-mantle thermal structure. The former represents the crustal thickness, whereas the latter is a temperature isothermal surface of the crust (Wang, 2015). There is a relationship between these two interfaces and heat flow. The depth map of the Moho generated by the inversion of the gravity and magnetic data shows that the depth of the Moho in Guizhou Province is 34–46 km in Fig. 6 (Qu et al. 2019), while 38 km to 48.5 km was obtained through the inversion of the Parker density interface (Wu et al. 2016). The Moho depth by using the above method is high in the east and low in the west, reflecting that the crust tends

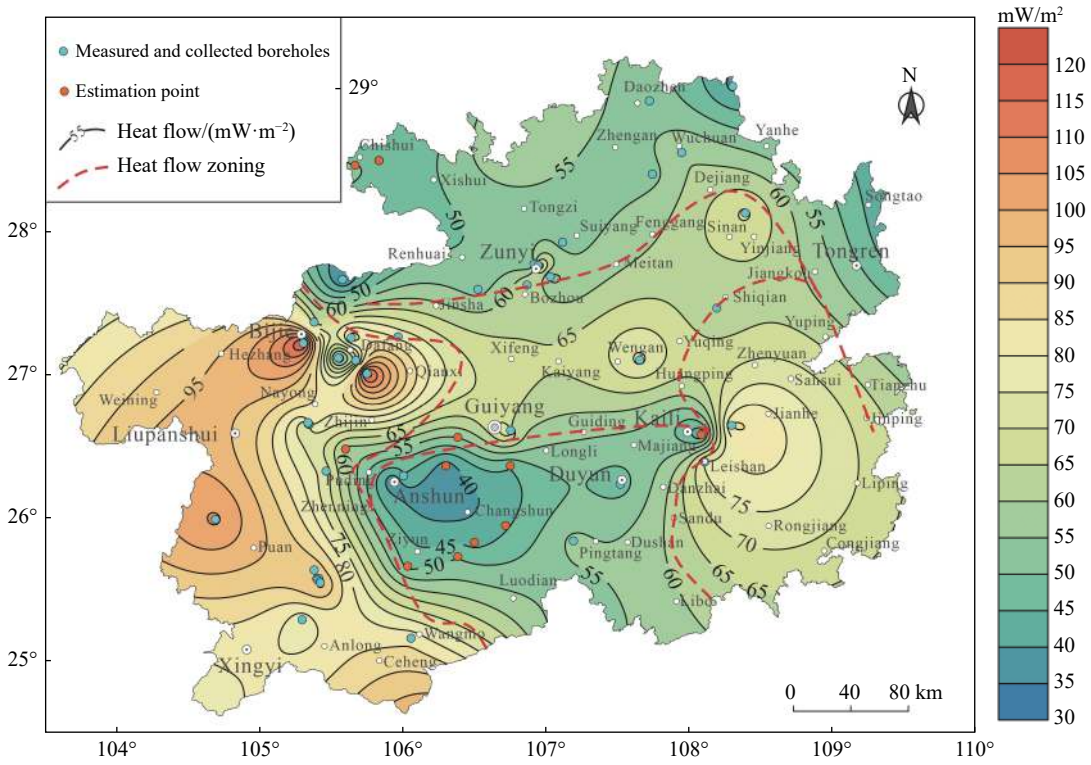

Fig. 5 Contour map of terrestrial heat flow in Guizhou Province

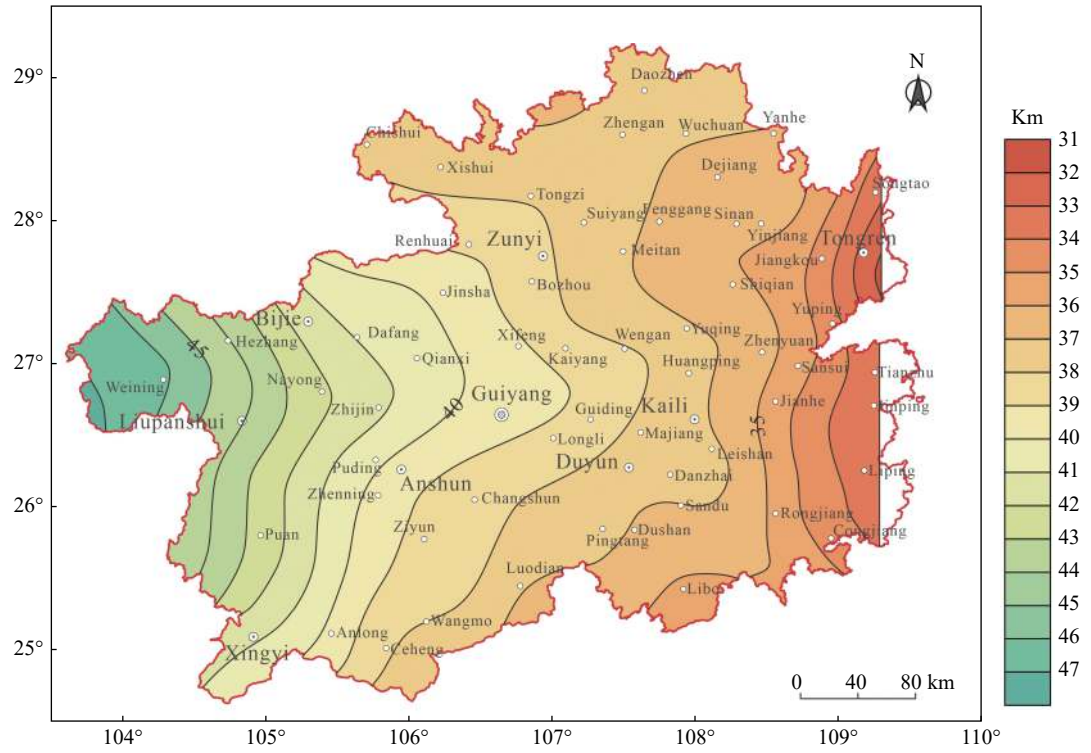

Fig. 6 Map of Moho depth in Guizhou Province (modified from Qu et al. 2019)

to gradually thicken from east to west in Guizhou. As the depth map of Moho surface and heat flow distribution show (Fig. 5 and Fig. 6), the heat flow values are mostly high where Moho surface is deep and low where the Moho surface is shallow, and there is a positive correlation between them.

The depth map of the Curie surface in Guizhou in Fig. 7 (Xiong et al. 2016) shows that the Curia surface in the west is uplifted, with a depth of 20–30 km, while the Curie surface in the east is depr-

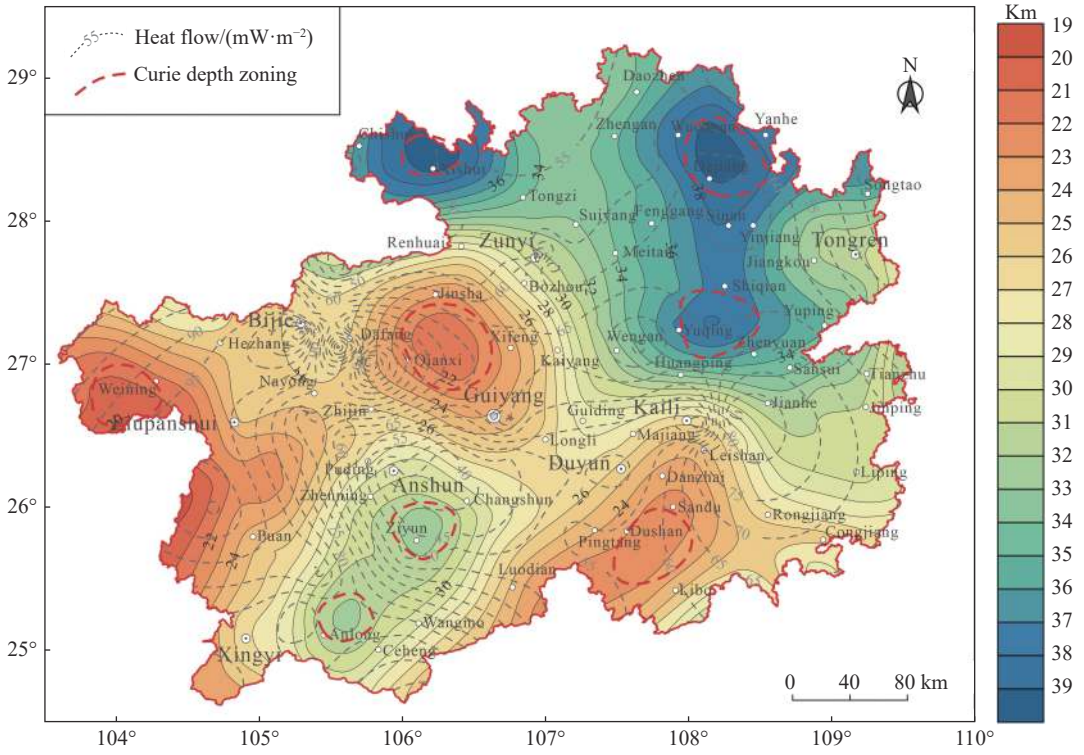

Fig. 7 Map of depth of Curie in Guizhou Province (modified from Xiong et al. 2016)

essed, with a depth of 26–38 km. Generally, the depth of the Curie surface gradually decreases from northeast to southwest and presents a banded distribution. Moreover, the Curie surface in areas such as Qianxi, Dushan, and Weining shows cloddy convexity, whereas the Curie surface in areas such as Ziyun, Anlong, Dejiang, Yuqing, and Xishui show cloddy depression. As shown in the depth map of the Curie surface and the distribution of geodetic heat flow (Fig. 7), the heat flow value is generally high in the shallow areas of the Curie surface, whereas the heat flow value tends to be low in the deep areas of the Curie surface, except for some local areas, which may be caused by the lack of local heat flow points or other factors. According to the relationships of the heat flow distribution characteristics with the Moho and the Curie surface, the heat flow values are generally high in areas with deep Moho and shallow Curie surface and lower in areas with shallow Moho and deep Curie surface.

4.2 Relationship between Emeishan basalts and geothermal flow

Terrestrial heat flow values are important parameters reflecting the thermal structure of the crust and mantle. In this paper, a scatter diagram of the regional heat flow values in the Emeishan large igneous province (ELIP) was created using the heat flow data of the whole land area of China (Wang and Huang, 1990), the estimated heat flow points in Guizhou (Wang et al. 1990), and the heat flow data calculated in this study (Fig. 8a). This diagram reflects the influence of ELIP on heat flow distribution patterns of Guizhou.

The heat flow data of the Panxi, Yunnan, and Sichuan basins have high quality and are defined as Class A (Wang and Huang, 1990). In the present study, the measured and collected data were reprocessed and the derived thermal conductivity datasets are considered more representative of the actual geological conditions of Guizhou, which were then used for the calculation and the result heat flow data generally have a better quality as Class C. Wang et al. (1990) used the temperature data of the borehole bottom or the thermal conductivities of neighboring boreholes to calculate heat flow data in Guizhou. Although the heat flow values were estimated, they still provided some information on the distribution of heat flow in areas far from the ELIP center. The scatter diagram of heat flow values in the ELIP region (Fig. 8a) shows that the heat flow is high in the inner and middle zones of the ELIP and but gradually decreases with the distance from the ELIP center (Jiang et al. 2018). The average values of heat flow in the inner, middle, and outer zones are 75.56 mW/m^2, 75.18 mW/m^2 and 59.15 mW/m^2, respectively. In addition, the heat flow values are gene-

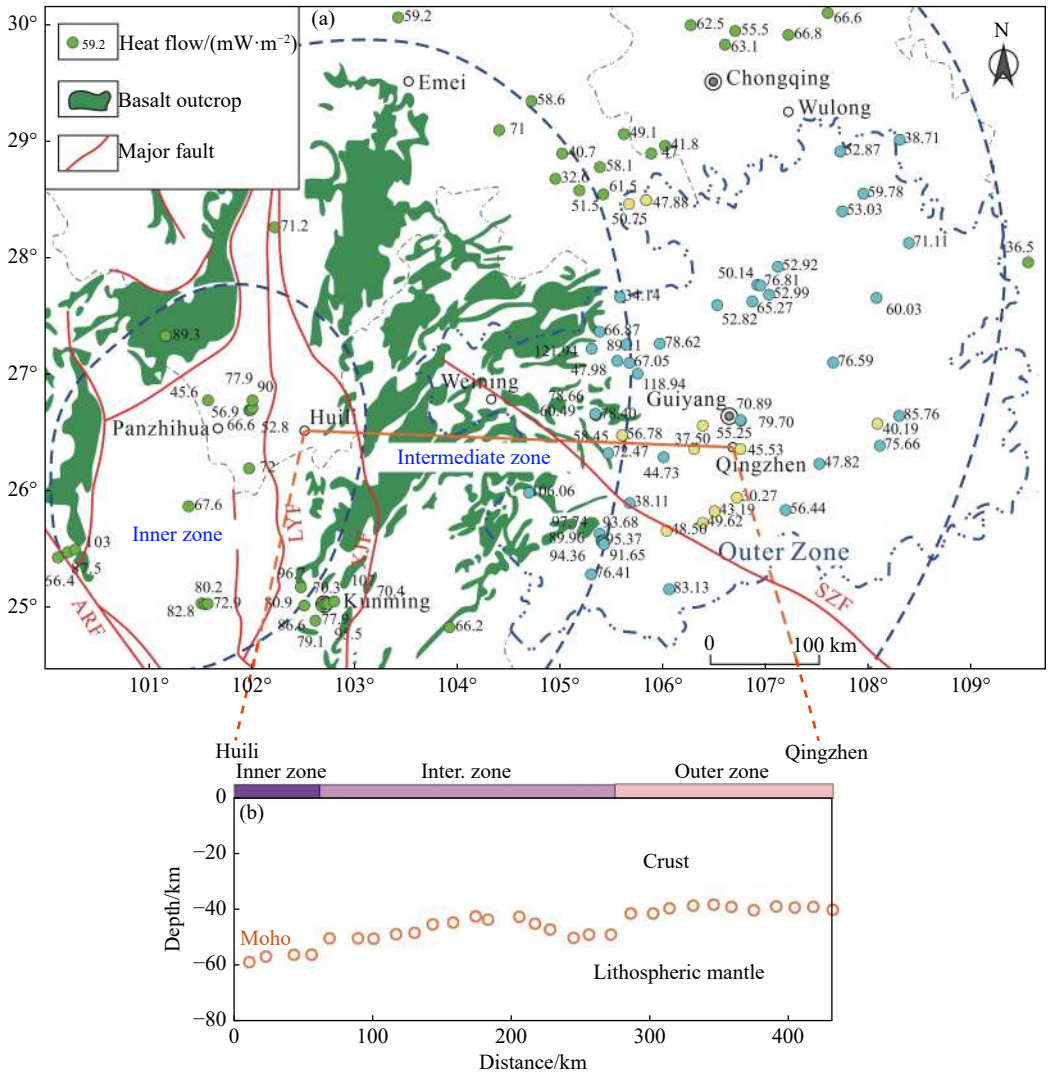

Fig. 8 (a) Map of Emeishan large igneous province and regional thermal flow dispersion. (b)Thermal lithospheric thickness of the Huili-Qingzhen transect (modified from Jiang et al. 2018)

Notes: Blue heat flow value points are calculated in this paper. Yellow heat flow value points are quoted from Wang et al. (1990). Green heat flow value points are quoted from Wang and Huang (1990). The blue dash lines represent the boundaries of the inner, intermediate, and outer zones of the ELIP defined by He et al. (2003). ARF: Ailaoshan-Red River slip fault; LYF: Lvzhijiang-Yuanmou Fault; XJF: Xiaojiang Fault; SZF: Shuicheng–Ziyun Fault

rally high near the NS-strike faults in the region, indicating that the NS-strike faults not only control the distribution of Emeishan basalts but also influence the distribution of heat flow (Fig. 8a).

According to previous research, there are three main controlling factors of the heat flow distribution pattern in the ELIP area. One is the large-scale Late Paleozoic Emeishan basaltic magma. The area close to the Emeishan basaltic eruption area has relatively high heat flow values (~70 mW/m^2), reflecting the thermal effect of magmatic activities. In addition, after the large-scale volcanism of the Emeishan mantle plume, a phase of large-scale and long-duration acid magma intrusion and eruption activities occurred; these acid magma activities have a close genetic connection with the Emeishan basalts, and the acid magmas may be eutectic products to the crust during the uplift of basaltic magmas (Lu, 1996). The distribution of intermediate-acid concealed bodies in western Guizhou, delineated using heavy magnetic anomalies, corresponds to the acid magma activities (Wang et al. 2020). The radiogenic heat production of the intermediate-acid bodies may have contributed to the heat flow.

The second factor is the upwelling of the mantle plume. The mantle plume extrudes the continental lithosphere, tending to cause magma bodies to enter the crust or the magmatic diapirs to form at the bottom of the crust in Fig. 9a (Feng et al. 2021). This process may cause a large thermal anomaly to penetrate the overlying crust. The magmatic dia-

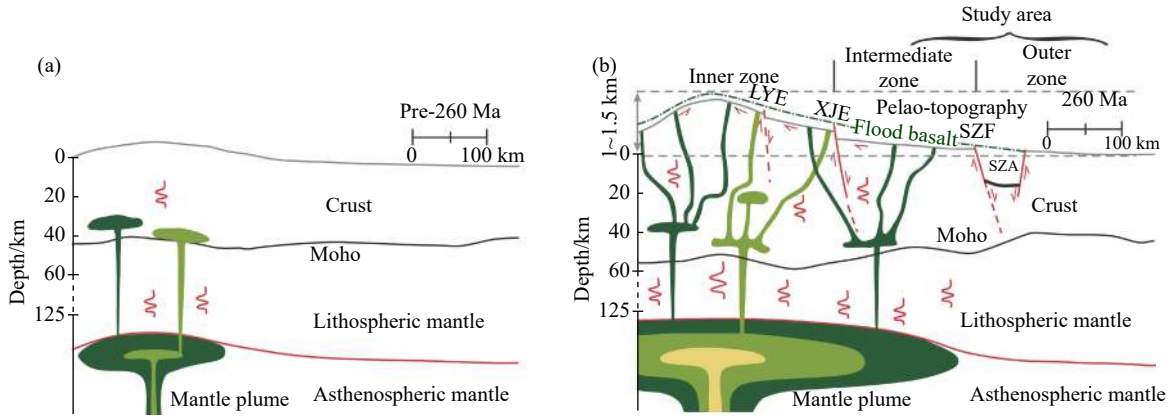

Fig. 9 Conceptual model for (a) early magmatic underplating by a mantle plume (modified after Feng et al. 2021); (b) progressive magma emplacement at depth, topographic uplift in the Emeishan LIP (modified from Feng et al. 2021; Chen et al. 2015)

Notes: LYF: Lvzhijiang-Yuanmou Fault; XJF: Xiaojiang Fault; SZF: Shuicheng–Ziyun Fault; SZA: Shuicheng-Ziyun Aulacogen

pirs can also lead to the vertical uplift of the upper crust through physical and chemical effects. Accordingly, hot magmatic bodies keep rising until they erupt at the surface (Fig. 9b), causing differential dome-shaped uplifts of more than 1 000 m in the inner zones and over 400 m in the middle zones (He et al. 2003). This process has produced an extensional tectonic setting and has activated some large regional faults (Chen et al. 2015) with depths of tens of kilometers which often connect to the mantle, providing thermal convection conditions. Structures and magmatic bodies may have caused the differential distribution of heat flow within the Emeishan basalts region.

The third factor is the mantle plume activities. The formation of the ELIP is related to the upwelling of mantle plumes, the fact that mantle plume materials impact the lithospheric basement, and the extensive magma diapirs. These activities are destructive of the lithosphere, as they cause lithospheric thinning and crustal thickening (Jiang et al. 2018; Shellnutt, 2014; Sun et al. 2010). In addition, geophysical studies have shown that although mantle temperature anomalies and mantle plume upwelling do not exist at the bottom of the lithosphere in the Emeishan basaltic region currently (He et al. 2014), Emeishan mantle plume could still affect the inner and middle zones of the relatively thin lithosphere where the heat flow are found to be high. Cross section showing the inner, middle, and outer zones from east to west in Huili-Qingzhen area and lithospheric thickness are presented in Fig. 8a, Fig. 8b and Fig. 9b. The lithospheric thickness gradually increases and the crustal thickness gradually decreases from the inner and middle zones outward. The change in crustal thickness may affect the heat flow distribution, but the additional surface heat flow resulting from the deep basaltic layer of the crust contributes little. Therefore, the lithospheric factor of the basaltic layer has limited influence. In addition, diapirs cause lateral emplacement of mantle plume material and crust, leading to the formation of basal laminated intrusions, which may also have some influence on heat flow.

4.3 Relationships between structures and terrestrial heat flow

Based on tectonic deformation, sedimentary rocks, geophysics, geochemistry, magmas, earthquakes, thermal springs, and deposit indicators, Dai et al. (2013) inferred 10 deep faults (Fig. 10) extending in four directions with lengths of from ~60 km to ~520 km. These deep faults are mostly lithospheric faults, and generally cut through the simasphere and cause the ultramafic magmas in the upper mantle to rise along the faults, moniliform and banded ultramafic rock bodies, earthquakes, hot springs, and hydrothermal deposits could be formed and distributed along the fault zones. Since regional deep faults are considered to have rock, mineral, and thermal conductivity (GSGP, 2017), the intertwined and overlapping parts of the concealed deep faults tend to be areas with high heat flow values.

The concealed deep faults not only connect to the heat source in the mantle but also obliquely intersect with the NE-, NNE-, and NS-strike active faults. Therefore, they are direct channels for the transfer of heat flow from deep to shallow parts of the Earth. As a result, the heat flow in Guizhou is partly controlled by both deep faults and shallow active faults (Chen, 2021). For example, as seen in Fig. 10, the Sinan-Yinjiang area, under the control of the concealed Muhuang-Guiyang-Pu' an deep

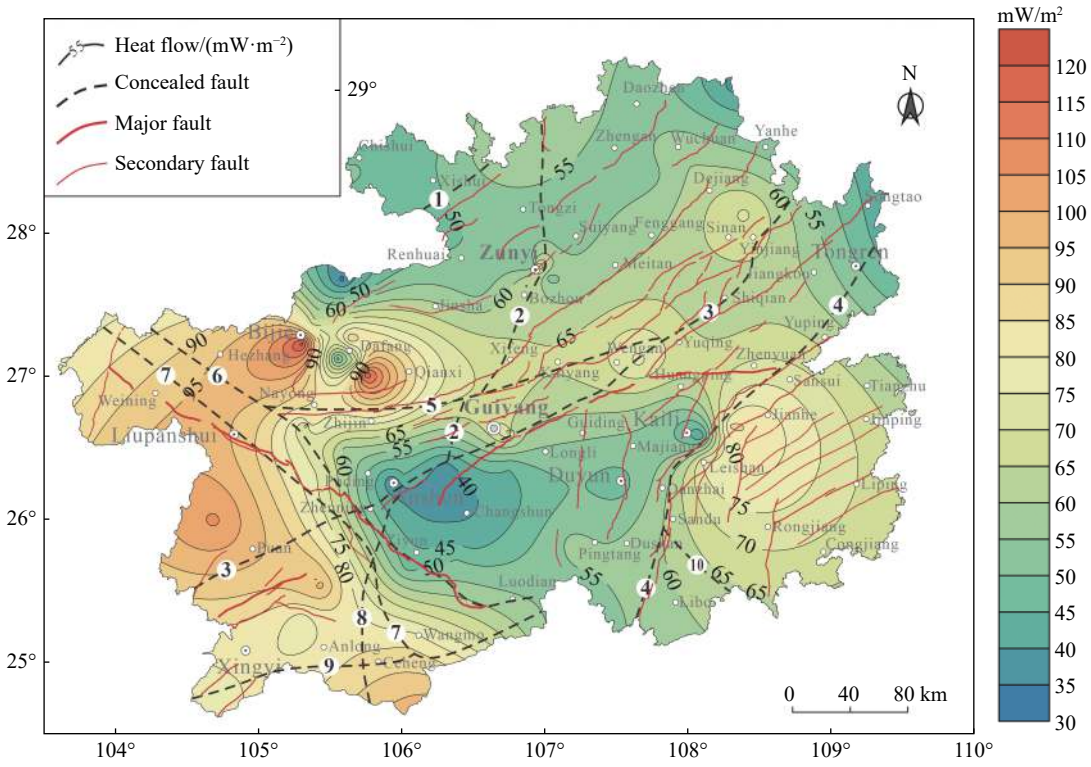

Fig. 10 Geological formations and heat flow distribution in Guizhou Province (hidden faults cited in Dai et al. 2013)

Notes: ①Hao-tan fault; ②Yangdeng-Zunyi-Weicheng fault; ③Muhuang-Guiyang-Pu'an fault; ④Yuping-Shidong-Sandu fault; ⑤Nayong-Kaiyang fault; ⑥Yadu-Ziyun fault; ⑦Shuicheng-Wangmu fault; ⑧Longgong-Zhenfeng fault; ⑨Mudai fault; ⑩Yanggong fault

fault and the Sinan-Baimadong strike-slip fault, is a region with high heat flow values. Similar conditions can be found in the Jianhe-Leshan area, controlled by the concealed Yuping-Shidong-Sandu deep fault and the Gedong active fault; the Weining-Liupanshui-Hezhang area, controlled by the Yadu-Ziyun, Shuicheng-Wangmu, and Shuicheng-Ziyun-Luodian faults. Comparted with the southern section of the Yadu-Ziyun between Wangmu and Luodian, the northwestern section of the area has no extenisvely developed faults (Mao et al. 1997) and thus has lower heat flow values.

5 Conclusions

Based on the measurement and characterization of the heat flow in Guizhou Province, the following conclusions can be made: (1) Most of the thermal conductivities obtained in this study are 2.0–5.0 W/(m·K), with an average of 3.399 W/(m·K). The thermal conductivities of rocks are in the order of sandy mudstones < siltstones < limestones < marls < tuffs < siliceous limestones < slates< fine-grained sandstones < dolomites < argillaceous dolomites. (2) The heat flow values in Guizhou range from 30.27 mW/m^2 to 157.55 mW/m^2, with an average of 65.26 ± 20.93 mW/m^2, which is slightly higher than the average heat flow of whole land area in China. The heat flow values in Guizhou are high in the east and west and low in the north and south, presenting dumbbell-shaped distribution. (3) The factors influencing the regional heat flow include the Moho, the Curie surface, the Emeishan basalts, and geological structures. There is a correlation between the heat flow values and the depths of the Moho and the Curie surface. The Emeishan basalts dominated the basic pattern of heat flow distribution in Guizhou via the following activities: The reflective heat production of both the erupted basaltic magmas and the late intermediate-acid intrusions, the formation of dome-shaped uplifts at the bottom of the magmatic diapirs, the activation of some large regional faults that can provide thermal convection conditions by the dome-shaped uplifts, and the lithosphere thinning, crustal thickening, and lateral emplacement caused by the upwelling of mantle plumes. In addition, regional active faults and concealed deep faults jointly control the heat transfer channels and further influence the heat flow in Guizhou.

Acknowledgements

This work was supported by the China Geological

Survey Project (Grant No. DD20190128; Grant No. DD20221676) and Basic Research Operations Project of the Institute of Hydrogeology and Environmental Geology, Chinese Academy of Geological Sciences (SK202212).

References

Ban WT, Duan XQ, Yang Q, et al. 2018. A study of the occurrence law of zonal thermal reservoirs in the Gedong area of Guizhou. Geology and Exploration, 54(2): 0366-0375. (in Chinese)

Chen MX, Huang GS, Xiong LP, et al. 1988. Geothermics of North China. Beijing: Science Press: 61-70. (in Chinese)

Chen P, Zhang BM, Jin B. 2014. Heat-reservoir structure study and its significance of Langgong scenic spot in Huangguoshu, Guizhou. Guizhou Geology, 31(4): 318-322. (in Chinese)

Chen XY, Jiang ZJ, Xu HY, et al. 2022. Heat control mechanism and productivity optimization of artificial fracture zone structure of dry hot rock in Gonghe Basin. Hydrogeology & Engineering Geology, 49(1): 191-199. (in Chinese)

Chen Y, Xu Y, Xu T, et al. 2015. Magmatic underplating and crustal growth in the Emeishan Large Igneous Province, SW China, revealed by a passive seismic experiment. Earth and Planetary Science Letters, 432: 103-114.

Chen ZS. 2021. The formation mechanism of physiotherapy thermomineral water (hot spring) in guizhou and its effect on human health. Ph. D thesis. Guizhou: Guizhou University: 53-166. (in Chinese)

Dai CG, Qin SR, Chen JS, et al. 2013. Characteristics of deep concealed faults in Guizhou. Geological Science and Technology Information, 32(6): 1-13. (in Chinese)

Ding J, Xiang T, You B, et al. 2019. Analysis on geothermal resources prospecting in Dashan-Xinzhuang area, Xingren County, Guizhou Province. West-China Exploration Engineering, 10: 142-146. (in Chinese)

Duan QB, Song XQ, Meng FT, et al. 2015. Study on occurrence law of geothermal water in metamorphic rock area of eastern Guizhou. Groundwater, 37(4): 37-39. (in Chinese)

Fang SW, Li Q, Chen G, et al. 2020. Study on distribution characteristics of geothermal field in central and Eastern Bijie, Guizhou Province. West-China Exploration Engineering, 10: 130-134. (in Chinese)

Feng K, Xu S, Chen A, et al. 2021. Middle permian dolomites of the SW Sichuan Basin and the role of the Emeishan large igneous province in their origin. Marine and Petroleum Geology, 128(3-4): 1-18.

Furlong KP, Chapman DS. 2013. Heat flow, heat generation, and the thermal state of the lithosphere. Annual Review of Earth and Planetary Sciences, 41: 385-410.

GBBGMEDGP (Geological Brigade of Bure of Geology and Mineral Exploration and Development Guizhou Province). 2015. Report on well completion of CK1 geothermal exploration hole in Longjing geothermal water survey in Duyun City, Guizhou Province. 114 Geological Brigade of Bure of Geology and Mineral Exploration and Development Guizhou Province. (in Chinese)

GSGP (Geological Survey of Guizhou Province). 2017. Regional geologic annuals of Guizhou. Beijing: Geological Publishing House: 1-788. (in Chinese)

Grall C, Henry P, Tezcan D, et al. 2012. Heat flow in the Sea of Marmara Central Basin: Possible implications for the tectonic evolution of the North Anatolian fault. Geology, 40(1): 3-6.

Guo C, Qin Y, Lu L. 2018. Terrestrial heat flow and geothermal field characteristics in the Bide-Santang basin, western Guizhou, South China. Energy Exploration & Exploitation, 36(5): 1114-1135.

He B, Xu Y, Chung S, et al. 2003. Sedimentary evidence for a rapid, kilometer-scale crustal doming prior to the eruption of the Emeishan flood basalts. Earth and Planetary Science Letters, 213(3-4): 391-405.

He C, Santosh M, Wu J, et al. 2014. Plume or no plume: Emeishan Large Igneous Province in Southwest China revisited from receiver function analysis. Physics of the Earth and Planetary Interiors, 232: 72-78.

He L. 2015. Thermal regime of the North China Craton: Implications for craton destruction. Earth-Science Reviews, 140: 14-26.

Hou DG. 2016. Research on reservoir characteristics and recoverability of CBM resources in Songhe mine field, Guizhou province. M.S. thesis. Xuzhou: China University of Mining and Technology: 21-51. (in Chinese)

Hu S, He L, Wang J. 2000. Heat flow in the continental area of China: A new data set. Earth and Planetary Science Letters, 179(2): 407-419.

Jiang G, Hu S, Shi Y, et al. 2019. Terrestrial heat flow of continental China: Updated dataset and tectonic implications. Tectonophysics, 753(20): 36-48.

Jiang GZ, Gao P, Rao S, et al. 2016. Compilation of heat flow data in the continental area of China (4th edition). Chinese Journal of Geophysis, 59(8): 2892-2910. (in Chinese)

Jiang Q, Qiu N, Zhu C. 2018. Heat flow study of the Emeishan large igneous province region: Implications for the geodynamics of the Emeishan mantle plume. Tectonophysics, 724-725: 11-27.

Li YL, Yu CS, Jiang ZC, et al. 2021. An experimental study of heating tail water treatment of the Lindian geothermal fields in the Northern Songnen Basin. Hydrogeology & Engineering Geology, 48(1): 188-194. (in Chinese)

Liu F, Wang GL, Zhang W, et al. 2020a. Terrestrial heat flow and geothermal genesis mechanism of geothermal resources in northern Ningdu County, Jiangxi Province. Geological Bulletin of China, 39(12): 1883-1890. (in Chinese)

Liu Y, Qiu N, Li H, et al. 2020b. Terrestrial heat flow and crustal thermal structure in the northern slope of Tazhong uplift in Tarim Basin. Geothermics, 83: 101709.

Lu JR. 1996. Dynamical characteristics of the Emei Mantle Plume. Acta Geoscientia Sinica, 17(4): 424-438. (in Chinese)

Lu LL. 2014. Differentiation and geological controls of modern geothermal field in Bide-Santang basin. M. S. thesis. Xuzhou: China University of Mining and Technology: 29-41. (in Chinese).

Lu LL, Qing Y, Guo C. 2013. Modern geothermal field and coal seam heating temperature in Buzuo exploration area, Western Guizhou. Coal Geology of China, 25(10): 12-17. (in Chinese)

Mao JQ, Zhang QH, Gu SY. 1997. The geological characteristics and tectonic evolution of Shuicheng fault subsidence. Journal of Guizhou University of Technology, 26(2): 1-6. (in Chinese)

Mao X, Li K, Wang X. 2019. Causes of geothermal fields and characteristics of ground temperature fields in China. Journal of Groundwater Science and Engineering, 7(1): 15-28.

Mu ZM, Wu L. 2021. Genetic analysis of hot mineral water in ZK2 geothermal well, Zhongba, Shiqian, Guizhou. West-China Exploration Engineering, 8: 131-136. (in Chinese)

Pollack HN, Hurter SJ, Johnson JR. 1993. Heat flow from the Earth's interior: Analysis of the global data set. Reviews of Geophysics, 31(3): 367-280.

Qu NN, Li JB, Zhang XJ, et al. 2019. Study of deep structural feature in Guizhou based on gravity and magnetic data. Progress in Geophysics, 34(5): 1785-1793. (in Chinese)

Rolandone F, Lucazeau F, Leroy S, et al. 2013. New heat flow measurements in Oman and the thermal state of the Arabian Shield and Platform. Tectonophysics, 589: 77-89.

Shellnutt JG. 2014. The Emeishan large igneous province: A synthesis. Geoscience Frontiers, 5: 369-394.

Song XQ, Jiang M, Peng Q, et al. 2019. Thermal property parameters and influencing factor analysis of main rock strata in Guizhou province. Acta Geologica Sinica, 93(8): 2092-2103. (in Chinese)

Song XQ, Peng Q, Xia YL. 2012. Estimation of reservoir temperature and circulation depth of geothermal water of SK08-2 well in Laofenzui metamorphic rock area of Wengan city. Water Saving Irrigation, 10: 24-26. (in Chinese)

Sun Y, Lai X, Wignall PB, et al. 2010. Dating the onset and nature of the Middle Permian Emeishan large igneous province eruptions in SW China using conodont biostratigraphy and its bearing on mantle plume uplift models. Lithos, 119(1-2): 20-33.

Tian XL. 2016. Occurrence and development of geothermal water in Shiqian fracture. Acta Geologica Sichuan, 36(4): 623-626. (in Chinese)

Tu MJ, Li Q, Yi SY. 2019. Study on the occur-

rence condition of geothermal in Leishan, Guizhou. West-China Exploration Engineering, 7: 154-156. (in Chinese)

Wang GL, Lin WJ, Zhang W, et al. 2018. Geothermal Records of China (Southwest Volume II). Beijing: Science Press: 499-525. (in Chinese)

Wang GL, Wang WL, Zhang W, et al. 2020. The status quo and prospect of geothermal resources exploration and development in Beijing-Tianjin-Hebei region in China. China Geology, 3: 173-181.

Wang JY. 2015. Geothermics and its applications. Beijing: Science Press: 56-122. (in Chinese)

Wang JY. Huang SP. 1990. Compilation of heat flow data in the China continental area (2rd edition). Seismology and Geology, 12(4): 351-366. (in Chinese)

Wang J, Huang SY, Huang GS, et al. 1990. Basic characteristics of the Earth's temperature distribution in China. Beijing: Geological Publishing House: 1-231. (in Chinese)

Wang J, Wang JA, Shen JY, et al. 1995. Heat flow in tarim basin. Earth Science-Journal of China University of Geosciences, 20(4): 399-404. (in Chinese)

Wang L, Zhang JW, Chen GY, et al. 2020. Delineation of concealed intermediate-acidic pluton and significance of mineral prospecting in Guizhou province. Geology and Exploration, 20(4): 399-404. (in Chinese)

Wang MZ, Wang SY. 2007. Concerns of developing geothermal resources in Guizhou province and counter measure proposals. Guizhou Geology, 24(1): 9-12. (in Chinese)

Wang Z, Rao S, Xiao H, et al. 2021. Terrestrial heat flow of Jizhong depression, China, Western Bohai Bay basin and its influencing factors. Geothermics, 96: 102210.

Wu KB, Zeng GQ, Chen GX, et al. 2016. Deep structural features of Guizhou revealed by bouguer gravity anomaly. Geological Science and Technology Information, 35(1): 190-199. (in Chinese)

Wu L, Zhao L, Luo XG. 2012. Characteristics of geothermal field and estimation of heat flow in Wudang district of Guiyang. Site Investigation Science and Technology, 3: 41-43. (in Chinese)

Xing JS, Yang WR, Xing ZY, et al. 2007. Deep-seated structure characteristics of eastern China and its relation with metal mineralization-concentrated region. Earth Science Frontiers, 14(3): 114-130. (in Chinese)

Xiong LP, Hu SB, Wang JA. 1994. Analysis on the thermal conductivity of rocks from SE China. Acta Petrologica Sinica, 10(3): 323-329. (in Chinese)

Xiong LP, Hu SB, Wang JY. 1993. Terrestrial heat flow values in southeastern China. Chinese Journal of Geophysics, 36(6): 784-790. (in Chinese)

Xiong SQ, Yang H, Ding YY. 2016. Characteristics of Chinese continent Curie point isotherm. Chinese Journal of Geophysics, 59(10): 3604-3617. (in Chinese)

Yang RK, Luo W, Pei RW, et al. 2018. Distribution and fluids hydrochemistry characteristics of hydrothermal geothermal resources in Guizhou Province. Geological Survey of China, 5(2): 38-44. (in Chinese)

Yang RK, Wang Q, Yang LJ, et al. 2015. Investigation, evaluation and zoning of geothermal resources in Guizhou Province. Guizhou Geological Environment Monitoring Institute: 1-157. (in Chinese)

Yang YJ, Ding GL, Xu W, et al. 2020. Tracer test and geothermal resource quantity evaluation based on dynamic data in the Xiaotangshan area of Beijing. Hydrogeology & Engineering Geology, 47(5): 196-200. (in Chinese)

Yuan FG. 1997. Geotherm characteristic of the north suburb of Zunyi city. Guizhou Geology, 14(2): 175-178. (in Chinese)

Yuan YS, Ma YS, Hu SB, et al. 2006. Present-day geothermal characteristics in South China. Chinese Journal of Geophysics, 49(4): 1118-1126. (in Chinese)

Zhang BJ, ZhaoT, Li YY,et al. 2019. The hydrochemical characteristics and its significance of geothermal water in both sides of large fault: Taking northern section of the Liaokao fault in north China as an example. China Geology, 2: 512-521.

Zhang CW, Li Q. 2015. Research of geotemperature field distribution characteristics and influence factors in Zunyi area. Guizhou Science, 33(2): 65-70. (in Chinese)

Zhang J, Huang S, Zuo Y, et al. 2020. Terrestrial heat flow in the baiyinchagan sag, erlian

Basin, northern China. Geothermics, 86: 101799.

Zhang L, Chen G, Li Q, et al. 2014. Formation condition and exploration prospecting of geothermal water in central Zunyi of Guizhou. Guizhou Geology, 31(1): 60-66. (in Chinese)

Zhang YH, Li X, Xu ZX, et al. 2021. An analysis of the genesis and engineering influence of geothermal water in the Kangding tunnel site of the Sichuan-Tibet Railway. Hydrogeology & Engineering Geology, 48(5): 46-53. (in Chinese)

Zhu SY. 2020. Study on the characteristics of geothermal water occurrence and water and heat migration in Zhenfeng anticline. M. S. thesis. Guizhou: Guizhou University: 25-28. (in Chinese)